Real-Time Characterization of Neutron-Induced SEUs in Fusion Experiments at WEST Tokamak during D-D Plasma Operation

Jean-Luc Autran, Soilihi Moindjie, Daniela Munteanu, Martin Dentan, Philippe Moreau, Francis-Pierre P Pellissier, Jérôme Bucalossi, Gianluca Borgese, Victor Malherbe, Thomas Thery, et al.

Real-Time Characterization of Neutron-Induced SEUs in Fusion Experiments at WEST Tokamak during D-D Plasma Operation

J.L. Autran, S. Moindjie, D. Munteanu, M. Dentan, P. Moreau, F.P. Pellissier, J. Bucalossi, G. Borgese, V. Malherbe, T. Thery, G. Gasiot and P. Roche

***Abstract*—We conducted a real-time soft-error rate characterization of CMOS bulk 65 nm SRAMs subjected to fusion neutrons during deuterium-deuterium (D-D) plasma operation at WEST tokamak. The test equipment, installed in the experimental hall at several locations of the tokamak, was irradiated during machine shots by a flux of particles dominated by primary 2.45 MeV neutrons. Real-time neutron metrology, neutron spectrometry, complementary characterization with monoenergetic neutrons and Monte Carlo numerical simulations at both material and circuit levels have been also performed to analyze experimental data. Our results suggest that higher energy neutrons, simultaneously produced by deuterium-tritium (D-T) reactions due to triton burn up in the D-D plasma, play a significant role in the radiation response of the SRAMs for which multiple cell upsets are detected and cannot be attributed to D-D neutrons.**

***Index Terms*—Fusion, tokamak, deuterium-deuterium, deuterium-tritium, neutron, single-event effects, single-event upset, SRAM, CMOS, real-time experiment, neutron spectrometry, numerical Monte Carlo simulation, TIARA, Geant4.**

I. Introduction

MAGNETIC and inertial confinement fusion devices have been extensively studied for more than fifty years to develop a future carbon-free source of energy for humanity. Although different isotopes of light elements can be paired to achieve fusion, the deuterium-tritium (D-T) reaction has been identified as the most efficient for fusion devices. ITER, the International Thermonuclear Experimental Reactor, and future energy production devices, such as DEMO, the Demonstration Power Plant, will use the hydrogen isotopes deuterium and tritium to fuel the fusion reaction [1]. Deuterium-deuterium (D-D) nuclear fusion reactions will be therefore used to study, during their development and commissioning, the fusion device operation before introducing tritium fuel. Both D-D and D-T operations produce a high flux of energetic neutrons, creating a residual neutron field outside the reaction chamber [2]. All future fusion devices will contain a large amount of electronics for machine command control and diagnosis, which could be exposed to nuclear radiation and negatively affected by this environment. To prevent such situation, most equipment will be installed outside the radiation field, and only a limited amount of electronics will be exposed to radiation near the reaction chamber. This work, which is part of a study conducted by ITER on the effects on electronics of the radiation environment in certain areas of the ITER tokamak building, is a first tentative step to characterize neutron induced SEUs (Single Event Upsets) in SRAM memories [3] exposed to the radiation field in the vicinity of a nuclear fusion device. Like other recent works but using a nuclear fission reactor as the neutron source [4] [5], it aims to anticipate the reliability of ITER electronics when the machine will be in operation with nuclear plasma, by the year 2035. The experiment was conducted at WEST tokamak during a test campaign under D-D plasma operation. It is based on the use of a real-time soft-error rate (RTSER) testbench with CMOS bulk 65 nm SRAMs [6]. In the last decade, very long measurement campaigns in various natural environments allowed us to accurately determine the soft error rate (SER) of this technology, both for atmospheric neutrons and alpha particle emitters present as ultra-traces in the bulk of device materials. RTSER measurements during the WEST campaign have been combined with near real-time neutron monitoring and spectrometry to simultaneously characterize the neutron flux and energy distribution during machine shots. In order to understand the exact role played by 14 MeV neutrons emitted in D-T reactions due to triton burn-up in D-D plasma, complementary experiments were conducted at the Laboratoire de Physique Subatomique et de Cosmologie (LPSC) in Grenoble and at the Institut de Radioprotection et de Sûreté Nucléaire (IRSN) in Cadarache. The paper is organized as follows. In Section II, the different experimental setups and irradiation configurations are described. Section III reports the experimental measurements obtained at WEST tokamak, LPSC and IRSN. These results are analyzed and discussed in Section IV, in particular in the light of extensive numerical Monte Carlo simulations performed for monoenergetic neutrons from 1 MeV to 14 MeV by step of 1 MeV. Implications for electronics reliability of future power fusion machines are finally discussed in Section V.

Manuscript received July 16, 2021.

This work was partially supported by ITER Organization.

J.L. Autran, S. Moindjie and D. Munteanu are with Aix-Marseille Univ, Université de Toulon, CNRS, IM2NP, 13397 Marseille Cedex 20, France. (email : jean-luc.autran@univ-amu.fr)

M. Dentan is with ITER Organization, F-13067 Saint-Paul-lez-Durance, France.

P. Moreau, F.P. Pellissier and J. Bucalossi are with CEA-IRFM, Centre de Cadarache, F-13115 Saint-Paul-lez-Durance, France.

G. Borgese is with Defense and Security Business Unit - Big Science Area, Vitrociset S.p.A, Roma, Italy.

V. Malherbe, T. Thery, G. Gasiot and P. Roche are with STMicroelectronics, 850 rue Jean Monnet, F-38926 Crolles Cedex, France.

II. Experimental setup and irradiation facilities

A. Real-time setup

As stated in the introduction, our experiment is based on a well-known and proven RTSER testbench embedding CMOS bulk 65 nm SRAMs manufactured by STMicroelectronics, previously operating several years at altitude on the ASTEP (Altitude Single event effects Test European Platform) facility, underground at the Laboratoire Souterrain de Modane (LSM) and at sea level in Marseille [7] [8]. This experimental test equipment embeds 384 memory circuits (3,226 Gbit) manufactured by STMicroelectronics in CMOS 65 with fabrication processes based on a BPSG (Borophosphosilicate Glass)-free BEOL (Back-End-Of-Line) that eliminates the major source of ^{10}B in the circuits and drastically reduces the possible interaction between ^{10}B and very low (thermal) energy neutrons. The test chips contain 8.5 Mbit of single-port SRAM (without deep-Nwell) with a bit cell area of 0.525 µm^2. This SRAM was extensively characterized under different radiation (neutrons, heavy-ions, alpha-particles) and also numerically simulated in 3D using TCAD tools in previous studies [6] [7] [8] [9]. The technology core voltage is 1.2 V. The circuits have been directly soldered on six printed multi-layered motherboards vertically assembled in a single rack (see Fig. 1). The ensemble of the circuits was controlled and monitored using a high reliability FPGA-based tester and characterized several years at altitude, underground and at sea level. Details about the setup and previous RTSER experiments can be found in [10]. We recall here that our RTSER testbench is fully compliant with all the specifications of the Joint Electron Device Engineering Council (JEDEC) standard JESD89B [11]. After initializing the full memory plan with the considered test pattern, the tester searches for error in loop until an error is detected. This loop, which corresponds to a complete scan of the full memory plan ($6 \times 64 = 384$ devices), is performed one time every 2.5 s. When an error is detected, the tester reads and verifies the implicated circuit to determine the nature of the error. The test algorithm used for this dynamic testing allows detection of Single Bit Upset (SBU), Multiple Cell Upet (MCU), Single Event Functional Interrupt (SEFI) and Single Event Latchup (SEL) events. Current consumption of all power lines provided by the tester is monitored and logged during the test. All measurements have been conducted under nominal conditions: supply voltage of 1.2V, room temperature, checkerboard test pattern. Just before this work, the equipment has been continuously working since March 2015 in Marseille (sea level), showing a consolidated and stable soft-error rate equal to n-SER = 226 FIT/Mbit due to atmospheric neutrons (NYC conditions) and α-SER = 1148 FIT/Mbit due to internal chip radioactivity [10].

B. WEST tokamak

The main irradiation campaign for this work was conducted at WEST tokamak, in Cadarache (France) from December 2020 to January 2021. WEST (acronym derived from W – tungsten – Environment in Steady-state Tokamak) is an experimental nuclear fusion device (Fig. 2) operated by the IRFM (Institute for Magnetic Fusion Research) institute from CEA (French Alternative Energies and Atomic Energy Commission) [12]. Its 50 m^3 toroidal vacuum chamber is equipped with superconducting toroidal magnets which allow steady-state plasma operation under a magnetic field of 3.7 T. The previous configuration of the machine, named Tore Supra, was operated between 1988 and 2011. The upgrade to WEST in 2013-2016 transformed the tokamak from a limiter to a divertor configuration [13], a key-transformation to test and validate the divertor architecture and operation for ITER [14]. During the experiment, the test equipment has been placed in the facility hall of the WEST tokamak (Figs. 2, 3 and 4), successively at three positions (7 m, 6 m and 5.2 m from the center of the machine). In the following, after presenting the global experimental data obtained for these 3 positions, we will focus our analysis on the single events induced by the plasma neutrons at the position P_3 = 5.2 m (see Fig. 4), for which the test equipment has received the highest neutron fluence. This corresponds to the last period of the test campaign during which the machine operation was the most stable and efficient. The SRAM circuits with their upper face oriented towards the center of the machine, were placed in the equatorial plane of the tokamak thanks to a mechanical support. The computer controlling the experiment was placed in the machine basement, shielded from neutrons under a borated concrete slab (thickness 80 cm).

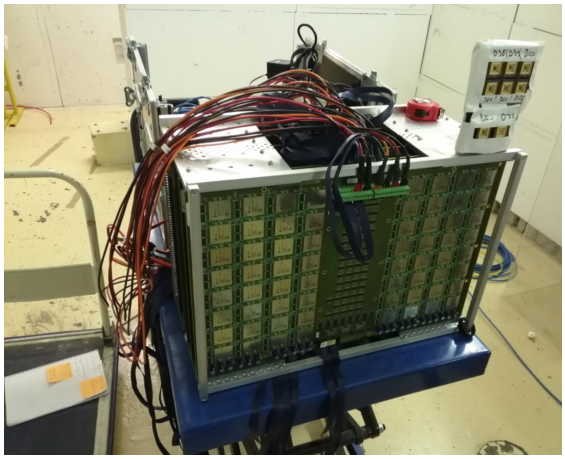

Fig. 1. Detail of the real-time soft-error rate testbench showing the measurement rack with 384 SRAM circuits in vertical position at GENESIS facility during the 14 MeV neutron irradiation campaign.

C. WEST neutron monitoring and spectrometry

The neutron counting and real-time monitoring during the machine shots was obtained from three groups of fission chambers positioned at 120° around the tokamak, near the vacuum chamber external wall. This monitoring system is a permanent and well proved set of equipment of the WEST installation, in operation for many years. The sensitivity of the fission chambers (adjusted using polyethylene moderator) is optimal for fusion neutrons, i.e., in the range 1-20 MeV. The calibration of the system was performed using a solid source of ^{252}Cf placed inside the tokamak chamber and moved step by step

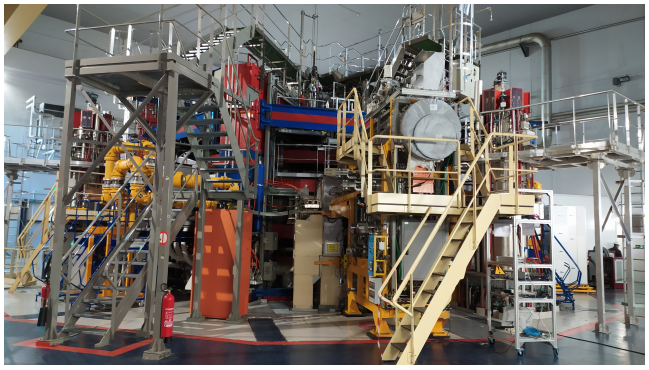

Fig. 2. General view of the WEST tokamak and the experimental hall. The support of the RTSER bench is visible at the bottom right of the image, partially behind the gateway stair.

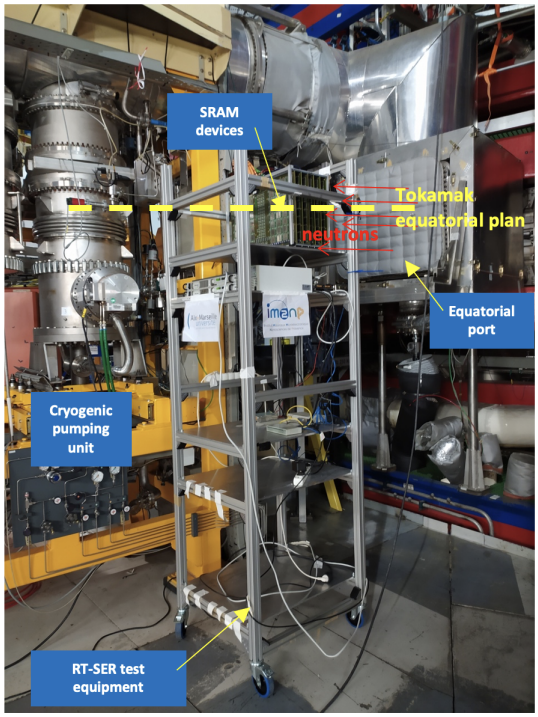

Fig. 3. Close-up view of the RTSER testbench installed on its support at the test position P_3 in front of the tokamak.

to cover the entire inner circumference of the torus. From this experimental determination of the response function of the ensemble tokamak+fission chambers, the detection system is able to estimate the total number of fusion neutrons produced in the whole tokamak chamber during a machine shot. We used this number to estimate the neutron fluence ($n.cm^{-2}$) at the level of our test bench (position P_3), considering the tokamak as a uniform toroidal source of neutrons (see Fig. 4 and Appendix). In complement to this neutron monitoring, we also performed neutron spectrometry during approximately one third of the machine shots. This characterization was performed using a commercial neutron spectrometer called DIAMON (Direction-aware Isotropic and Active neutron MONitor). This novel detection system is based on a polyhedral moderator body

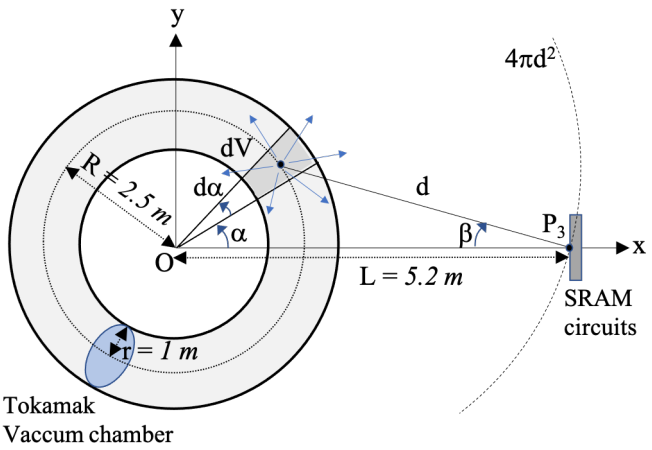

Fig. 4. Schematic top view of the tokamak with the definition of distances and angles. The position P_3 of the experimental setup is indicated.

made of high-density polyethylene (HDPE) which hosts a matrix of semiconductor-based thermal neutron sensors [15]. The instrument was carefully calibrated by its manufacturer at the neutron calibration facility of Politecnico di Milano using a ^{241}Am-Be source. During the measurements, the spectrometer was directly placed and aligned on the memory rack in order to characterize the neutron flux at the exact location of the irradiated circuits.

D. GENESIS facility at LPSC

In addition to the main experimental campaign conducted at WEST, we performed complementary measurements in May 2021 using a monoenergetic source of neutrons available at LPSC laboratory on the GENESIS (GEnerator of NEutrons for Science and IrradiationS) facility plaform [16]. GENESIS consists of an electrostatic accelerator of 220 kV called GENEPI2, delivering neutrons thanks to fusion reactions in a deuterated or tritiated target. The deuteron ions are created by an electron cyclotron resonance (ECR) compact source, designed and made at LPSC (accelerator and ion source division). Installed at the 220 kV HV terminal, it produces a continuous beam injected into an electrostatic column, analysed by a magnet and guided to the target. For our experiment, a tritiated target was installed, producing 14 MeV neutrons via the T(d,n)^{4}He nuclear reaction. The beam intensity was fixed to 100 μA (± 2%), giving a very stable neutron flux of $(2.1 \pm 0.1) \times 10^3$ $n.cm^{-2}.s^{-1}$ at the level of the test bench installed at a distance of 3 m from the solid target (see Fig. 1). This distance ensures that the printed boards, vertically positioned in front of the target, are uniformly and completely covered by the monoenergetic neutron beam.

E. AMANDE facility at IRSN

A second series of additional measurements has been obtained using a source of neutrons available at IRSN Institute on the AMANDE (Accelerator for Metrology And Neutron applications for external DosimEtry) facility. AMANDE is

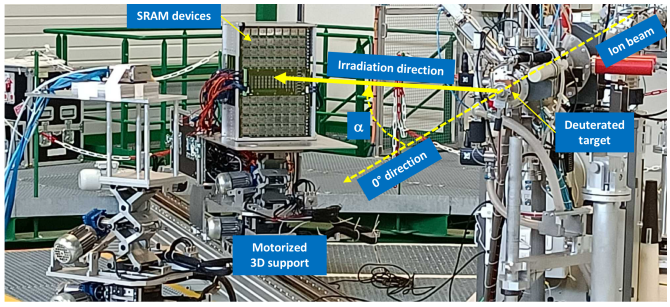

Fig. 5. General view of the AMANDE installation with the SER test bench in irradiation position at an angle of $\alpha = 50°$ with respect to the direction of the deuteron beam.

a metrology plaform that produces monoenergetic neutron reference fields as defined in the international standards ISO 8529 and ISO 12789. These neutron reference fields are used to calibrate radiation protection instruments and determine measuring instrument response as a function of neutron energy. The core of AMANDE is a 2 MV Tandetron ion accelerator producing proton or deuteron beams that interact with a deuterated or tritiated target in the same way as for GENESIS. The energy of the neutrons emitted from the target depends on beam and target properties but also varies with the emission angle in relation to the ion beam direction (see Fig. 5). This property can be used to change the energy of monoenergetic neutron fields without changing the energy of the ion beam. With emission angles of up to $\pm 150°$, the neutron energy range covered by the facility is 2 keV to 7.3 MeV and 12 MeV to 20.5 MeV. During the measurement campaign conducted at the end of July 2021, three neutron energies were selected: 0.48 MeV, 2.06 MeV and 13.94 MeV. The first value was chosen to estimate the neutron radiation response of the SRAM under test below 1 MeV, a domain never explored in previous accelerated experiments; the second value roughly corresponds to D-D neutron energy and the third value allows a direct comparison with results obtained at LPSC.

III. Experimental results

A. WEST tokamak operation and fusion neutrons

The WEST C5 SEE measurement campaign started on December 8, 2020 and finished on January 27, 2021 (50 days). It consisted in a series of 680 machine shots during which plasma conditions (with different characteristics: temperature, density, current) are met for D-D fusion following the two main reactions with equal probability of occurrence:

$$D + D \longrightarrow {}^{3}He(0.82MeV) + n(2.45MeV) \quad (1)$$

$$D + D \longrightarrow T(1.01MeV) + p(3.02MeV) \quad (2)$$

Once D-D fusion is correctly initiated at the beginning of a machine shot, the concentration of 1 MeV tritons (produced in the second D-D reaction) gradually increases in the plasma and renders possible D-T fusion:

$$D + T \longrightarrow {}^{4}He(3.52MeV) + n(14.07MeV) \quad (3)$$

This process is known as "triton burn up" and 14 MeV neutrons produced in D-T reactions occurring in deuterium discharges are called "triton burn up neutrons" (TBN) [17]. Note that in addition to these fusion neutrons emitted from the bulk of the plasma, some sporadic high energy photoneutrons can be emitted via the interaction of gamma rays with the plasma walls, these gammas being produced by the so-called runaway electrons during disruptions (a disruption is a fast, unstable event that leads to a sudden loss of plasma confinement; this phenomena is often accompanied with a sudden peak of neutrons at the plasma termination) [18].

Fig. 6 shows the distributions of the total number of neutrons produced during machine shots versus shot duration for all shots of the C5 campaign. Shots are ranging from 1 to 18 seconds in duration and from 10^8 to 10^{13} produced neutrons. They correspond to neutron fluences ranging from 10^2 to 10^6 $n.cm^{-2}$ at the place of the SRAM circuits. Note that in the following, all neutron fluences were deduced from WEST fission chambers using the procedure previously described in II.C. since these measurements, unlike those performed with the DIAMON spectrometer, were available for all machine shots. The cumulated neutron fluence reached at the end of the campaign for the exposed circuit was evaluated to be 5.6×10^8 $n.cm^{-2}$. The relationship between neutrons per shot and shot duration is not linear but the longest shots correspond to the highest quantities of produced neutrons. In Fig. 6, shots during which a SEU event have been detected in coincidence with the neutron flux are indicated in red. This evidences a link between the number of neutrons produced per shot and the occurrence of the single events: no SEU was detected for shots exhibiting fewer than 10^{11} neutrons. The vast majority of shots with SEU correspond to the shots during which the production of neutrons is high, typically above 10^{12} neutrons per shot.

All D-D and D-T neutrons (and also disruption photoneutrons) are transported outside the machine and produce, by absorption, reflection and attenuation mechanisms, a complex radiation field outside the machine. This radiation ambiance in the experimental hall is composed of thermal, low and high energy neutrons. Fig. 7 shows a typical full neutron spectrum measured during a machine shot by the DIAMON spectrometer. Two main peaks are well visible in this spectrum of neutron fluence rate per unit lethargy (the neutron fluence rate is plotted with the energy in log scale, having care of multiplying the fluence rate value for each bin by the median energy of the bin): the thermal peak below 0.1 eV and a high energy peak above 1 MeV. Thermal and low energy neutrons represent an important fraction of the neutron flux but their role is negligible in the SEE production mechanisms for the tested SRAM, not sensitive to thermal neutrons (BPSG-free process as reported in II.A). In the following, we focus of the high energy part of the spectrum, typically above 0.1 MeV, for which neutrons can play a role in the production of SEEs. The "high energy" peak around 1-2 MeV corresponds to D-D neutrons, initially emitted at 2.45 MeV in the plasma bulk and transported outside the tokamak chamber. Due to potential changes in the control parameters of the plasma and fusion conditions (imposed by the working program conducted by

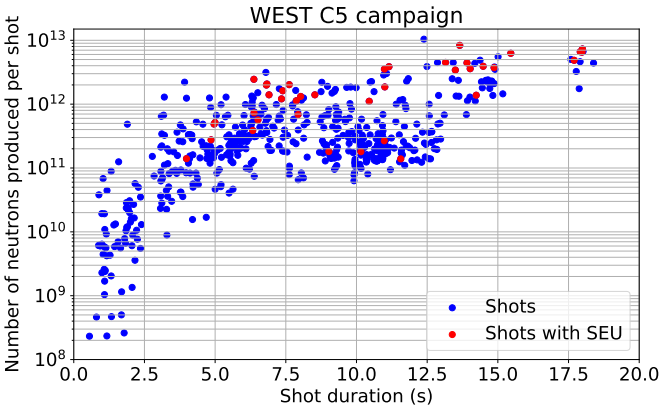

Fig. 6. Distribution of the number of neutrons produced during machine shots versus shot duration for all shots of the WEST C5 campaign. Machine shots during which a SEU event have been detected in coincidence with the neutron flux are indicated in red.

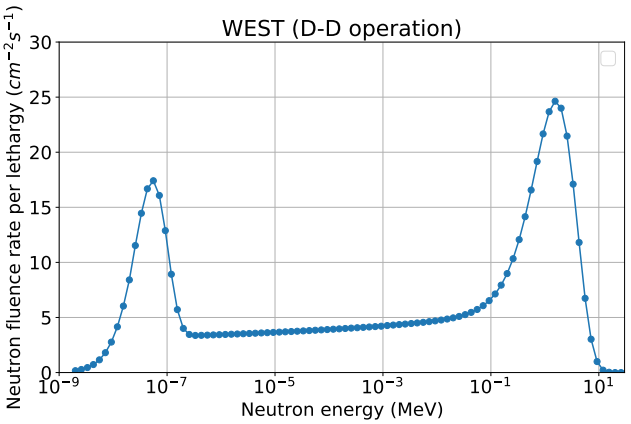

Fig. 7. Typical neutron spectrum measured with the DIAMON spectrometer during a machine shot.

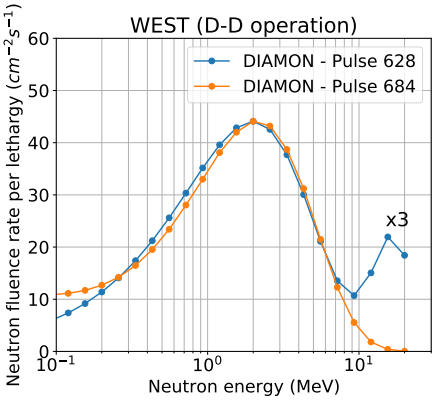

Fig. 8. Two neutron spectra measured with the DIAMON spectrometer during machine shots #628 and #684. y-values for the spectrum related to the pulse #628 have been multiplied by a factor $\times 3$.

CEA IRFM during the measurement campaign), the neutron fluence and flux changed from one machine shot to another, but neutron energy distribution remained broadly unchanged. The statistical analysis of 74 spectra measured at the position P_3 gives an average value of 1.35 MeV for the energy position of the maximum of the "high energy" peak with a standard deviation of 0.22 MeV. The FWHM for this peak is (3.1 $\pm$ 0.4) MeV. For a few measurements for which the acquisition was launched with a trigger delay to characterize the neutron flux emitted in the last seconds of a shot, as for the shot #628 in Fig. 8, a hump in the spectrum above 10 MeV was also detected. This hump corresponds to the signature of 14 MeV TBN neutrons, also transported and moderated through the tokamak structure. Qualitatively speaking, the triton concentration in the plasma increases gradually from the beginning to the end of a shot. The spectrum of pulse #628 shows a small hump around 12 MeV because it only caught the end of the pulse, when the triton/deuterium concentration ratio (T/D) is maximum. The spectrum of the other pulse (e.g. pulse #684), measured for the total duration of the pulse, integrates measurements made for T/D concentration ratios evolving from zero (at the beginning of the pulse) to a maximum value (reached at the end of the pulse). For this reason, the high energy part of the corresponding spectrum (such as pulse #684) appears as a spread of the main peak and not as a clearly separated hump. The main difficulty to experimentally resolve this second peak with the DIAMON spectrometer comes from the combination of this aspect of the measurement procedure with an intrinsic limitation of the DIAMON proprietary internal software used to reconstruct the neutron spectrum from raw measurements obtained with several detectors.

B. SEU measurements at WEST tokamak

For the whole duration of the C5 campaign, 54 SEU events for a total of 66 bit flips has been measured:

- On the one hand, 5 events including 4 single bit upsets (SBU) and 1 multiple cell upset (MCU) of multiplicity 3 (noted MCU(3)) have been recorded during the machine shutdown (nights, week-ends and end of year holidays) or during the machine stops for machine maintenance ($>$ 30 minutes) between consecutive sequences of machine shots.
- On the other hand, 49 events (42 SBU, 4 MCU(2) and 3 MCU(3)) have been detected in perfect coincidence with a shot, taking into account the duration of the reading/verification cycle of the test equipment.

For these 49 events induced by the machine operation, 41 of 49 have been observed after January 17, 2020, i.e., in the last ten days of the C5 campaign during which steady-state plasma conditions and a maximum D-D fusion efficiency have been obtained. In the following and unless otherwise indicated, we will consider these 41 events (36 SBU, 3 MCU(2) and 2 MCU(3)) for the analysis and discussion. This ensemble of events corresponds to 87.8% of SBU and 12.2% of MCU. Fig. 9 shows the bit flip occurrence as a function of neutron fluence for these events. A total of 48 bit flips is reached for a cumulated neutron fluence of 1.43×10^8 $n.cm^{-2}$ obtained after 1252 s (0.348 h) of machine operation (sum of all shot

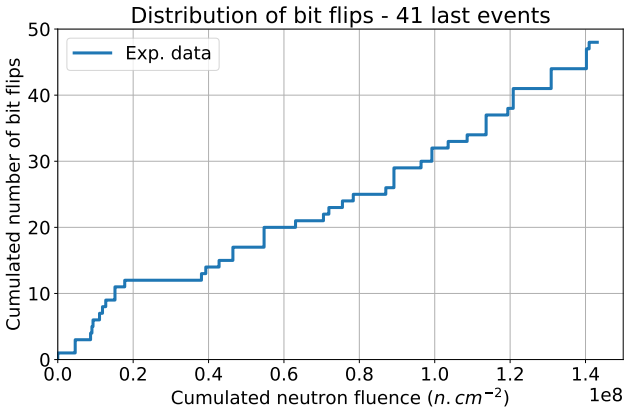

Fig. 9. Bit flip distribution as a function of the neutron fluence for the 41 last events detected during the WEST C5 campaign.

durations for this period). With respect to a reference neutron flux of 20 $n.cm^{-2}h^{-1}$, the tokamak radiation environment gives an acceleration factor of the real-time experiment equal to $AF = 2.06 \times 10^7$. The corresponding bit-flip soft-error rate under tokamak radiation is equal to n-SER = 4.3×10^7 FIT/Mbit and the bit-flip neutron cross section for the SRAM is evaluated to $\sigma_n = 9.9 \times 10^{-17}\ cm^2/bit$.

C. SEU measurements at GENESIS (LPSC)

At LPSC, the real-time setup was exposed to 14 MeV monoenergetic neutrons under a constant fluence rate of $(2.1 \pm 0.1) \times 10^3\ n.cm^{-2}s^{-1}$ up to a total neutron fluence of $(7.45 \pm 0.35) \times 10^7\ n.cm^{-2}$. At the end of this period, the system detected a cumulated number of 521 events (612 bit flips) including 461 SBU and 60 MCU: 31 MCU(2), 27 MCU(3) and 2 MCU(4). These results correspond to 88.5% of SBU and 11.5% of MCU events. Note that this event distribution in multiplicity is surprisingly very similar to the distribution observed at WEST. The corresponding bit flip neutron cross section for the SRAM is evaluated to $\sigma_n = (2.43 \pm 0.12) \times 10^{-15} cm^2/bit$.

D. SEU measurements at AMANDE (IRSN)

At IRSN, the real-time setup was successively exposed to 0.48 MeV, 2.06 MeV and 13.94 MeV monoenergetic neutrons. Table I summarizes the irradiation conditions, the metrology of the neutron flux (experimental uncertainties) and the number of detected SEU events characterized in terms of SBUs and MCUs. These results indicate about 86.6% of SBU and 12.4% of MCU events for 14 MeV neutrons. At 0.48 MeV, no MCU was detected and only 1 (for a total of 54 events) at 2.48 MeV. The evaluated bit flip neutron cross sections for the three neutron energies are also reported at the end of Table I.

We note that the measured cross section at WEST is half of the value measured here using 0.48 MeV neutrons. This result is a consequence of the distribution of the tokamak neutron flux dominated by low energy neutrons. Indeed, it must be recalled that the differential energy spectrum of the tokamak source is continuously decreasing with energy from thermal energy up to its maximum value around 10 MeV (this is not directly visible in the lethargic representation of Fig. 7). Even if the sensitivity of fission chambers used at WEST for neutron dosimetry is optimal for fusion neutrons in the range 1-20 MeV, these detectors also count a large part of lower energy neutrons that contribute to increase the measured neutron flux. The consequence of this integration of the neutron flux over a large energy domain is a value of the estimated bit-flip cross-section well below the cross-section values measured using mono-energetic neutron sources that leads to a factor of 2 between values measured at WEST and at AMANDE using 0.48 MeV neutrons.

TABLE I
SUMMARY OF MONOENERGETIC NEUTRON IRRADIATIONS AT AMANDE (IRSN)

Neutron energy (MeV)	0.48 ± 0.06	2.06 ± 0.31	13.95 ± 0.26
Fluence rate ($n.cm^{-2}.s^{-1}$)	1751 ± 571	1638 ± 992	3361 ± 81
Fluence ($\times 10^7 n.cm^{-2}$)	1.47 ± 0.48	1.45 ± 0.89	4.17 ± 0.1
SBU	9	34	239
MCU events	0	1 (*)	37 (**)
Total events	9	35	276
Total bit-flips	9	36	340
Bit-flip $\sigma_n (\times 10^{-15} cm^2/bit)$	0.18 ± 0.06	0.73 ± 0.47	2.41 ± 0.06

* A single MCU(2) ** 14 MCU(2), 22 MCU(3) and 1 MCU(7)

IV. Result analysis and discussion

The events observed during the whole campaign (50 days = 1200 h) are the result of two radiation sources working in parallel: the natural radiation background and the artificial machine environment. For the first one, the observations nicely agree with the neutron (226 FIT/Mbit) and alpha SER (1148 FIT/Mbit) measured in a previous study [10], even if the place (altitude 250 m) and the shield situation (building roofing) slightly changed from the point-of-view of atmospheric neutrons. Indeed, the number of expected events for 1200 h of exposure to natural radiation is $226 \times 3226 \times (1200/10^9) = 0.87 \approx 1$ for atmospheric neutrons and $1148 \times 3226 \times (1200/10^9) = 4.44 \approx 4$ for chip internal radioactivity, that corresponds to a total of 5 events. We effectively observed 4 SBU and 1 MCU not correlated with a machine shot, which exactly corresponds to the number estimated previously. But in absence of background spectrum for radiation when the tokamak is stopped, it is therefore not possible to say if these events are really due to natural radiation (shielding conditions may also changed) or if they are due to the residual radioactivity (activated materials) present in the tokamak hall.

For the artificial machine environment (WEST), composed of a mixture of very majority “low” energy (D-D) and minority “high” energy neutrons, the main issue is to try to determine the respective contributions of these two neutron categories in the observed occurrence of both SBU and MCU events.

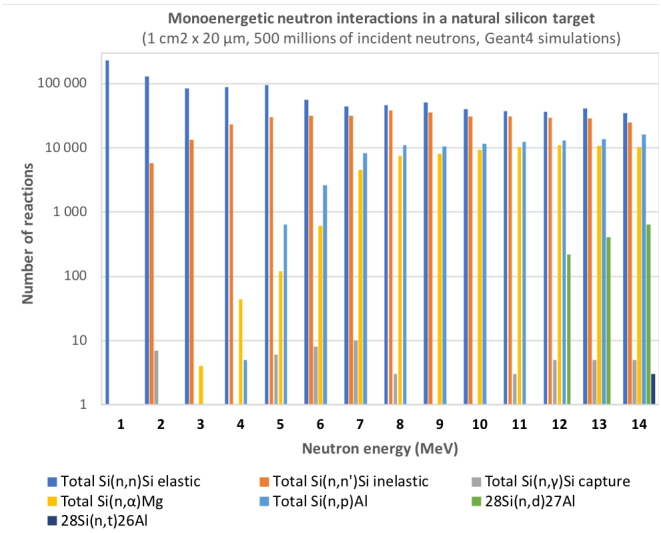

Fig. 10. Number of reactions resulting from the Geant4 simulation of the interactions of 5×10^8 of monoenergetic neutrons with a natural silicon target of 1 $cm^2 \times 20\mu m$ as a function of neutron energy.

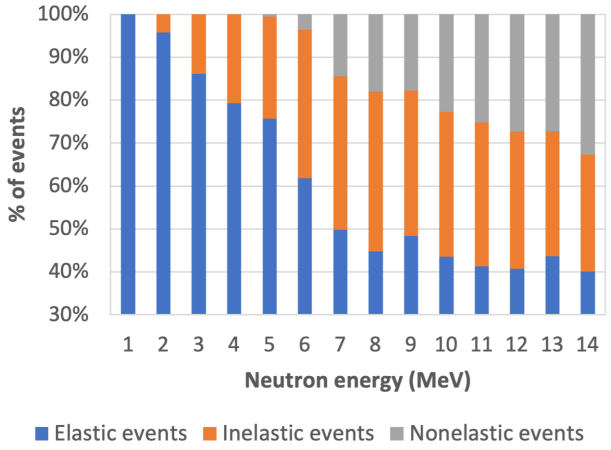

Fig. 11. Percentage of elastic, inelastic and nonelastic events calculated from Geant4 simulation results of Fig. 10 as a function of incident neutron energy.

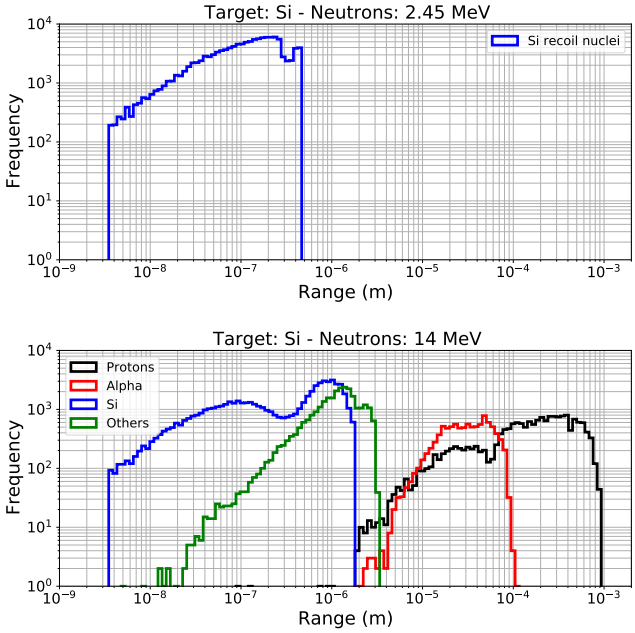

Fig. 12. Range distribution of Si recoils in silicon produced in n-Si interactions by 2.45 MeV (D-D) and 14 MeV (D-T) neutrons and deduced from Geant4 simulation (5×10^8 of monoenergetic neutrons, natural silicon target of 1 $cm^2 \times 20\ \mu m$).

To shed some light on this question, we performed a complementary numerical simulation study at both material and circuit level :

1) Following a methodology employed in various other studies [19] [20] [21], we first used the radiation transport code Geant4 [22] [23] to compute a complete set of interaction event databases of monoenergetic neutrons with a natural silicon target for neutron energies ranging from 1 MeV to 14 MeV by step of 1 MeV. These databases were then exploited to estimate the occurrence probability of elastic, inelastic and nonelastic events, as well as the energy, LET and range distributions of all secondaries produced in these different types of interactions.
2) These computed interaction event databases were also considered as input data for the numerical simulation of an array of 65 nm SRAM cells for the estimation of the circuit SER. These numerical simulations were performed using the Monte Carlo simulation code TIARA (Tool suIte for rAdiation Reliability Assessment) [24] [25].

A. Geant4 and SRIM simulations

Figs. 10 and 11 respectively show the distribution of elastic, inelastic and nonelastic events [26] and the number and percentage of events per reaction type resulting from the interactions of 500 millions of monoenergetic neutrons with a natural silicon target of 1 $cm^2 \times 20\mu m$. Below $\sim 5\ MeV$, only elastic and inelastic interactions occur, producing exclusively target recoil nuclei. For higher neutron energies, nonelastic interactions also occur and the proportion of elastic+inelastic interactions consequently decreases. At 14 MeV, this proportion is reduced to 70% and the remaining 30% correspond to nonelastic reactions producing secondary fragments. In addition to these results quantifying the events by their nature, we computed in Figs. 12 and 13 the range and the LET distributions of all secondaries produced in 2.45 MeV and 14 MeV neutron-silicon interactions. At 2.45 MeV, the produced recoil nuclei are characterized by very short ranges in the target, typically ranging from a few nanometers to $\approx 0.5\ \mu m$, a characteristic length that is largely inferior to the maximum distance ($0.79\ \mu m$) between two drain sensitive volume in the considered 65 nm SRAM topology with the test pattern used to initialize the logical state of each memory cell (checkerboard pattern). On the contrary, at 14 MeV, secondary fragments produced in nonelastic reactions, e.g., protons, alpha-particles and other secondary ions, are characterized by longer ranges

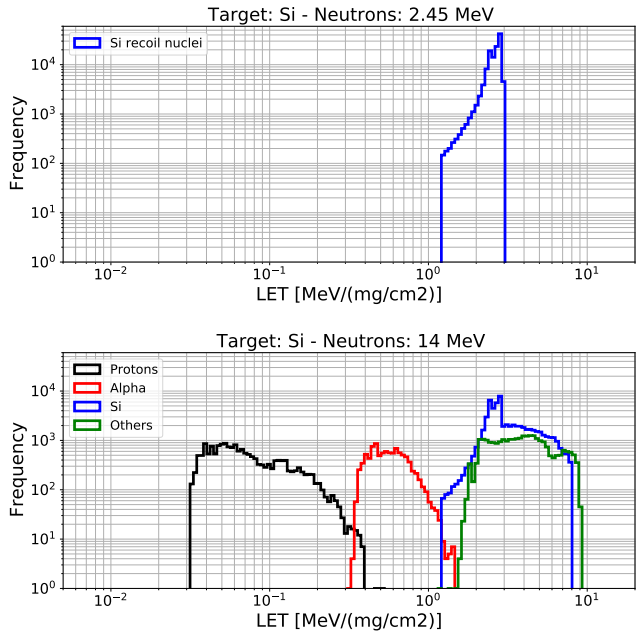

Fig. 13. LET distribution of Si recoils in silicon produced in n-Si interactions by 2.45 MeV (D-D) and 14 MeV (D-T) neutrons and deduced from Geant4 simulation (5×10^8 of monoenergetic neutrons, natural silicon target of $1\ cm^2 \times 20\ \mu m$).

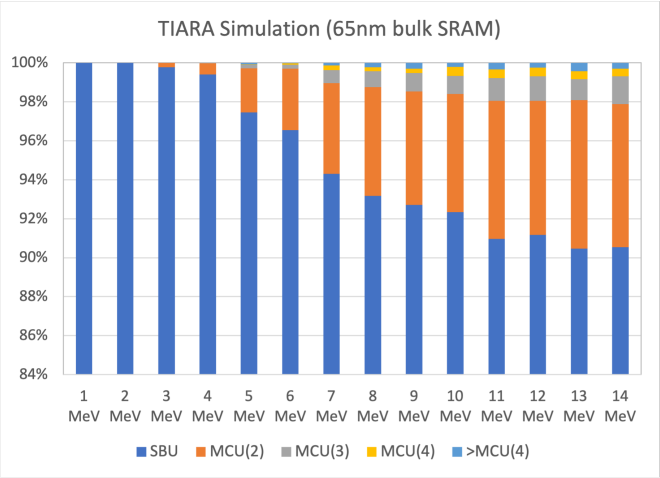

Fig. 14. Distribution of SBU and MCU events (in percents) obtained by TIARA simulation for the 65 nm SRAM subjected to neutrons from 1 to 14 MeV.

which can extend to nearly 100 µm for alpha-particles and up to 1 mm for protons. Despite lower LET values, these particles are likely to directly impact two or several neighboring sensitive drain volumes (or to pass in their immediate vicinity), a necessary condition to observe MCU events in absence of significant bipolar amplification (discussed below). We can conclude from these geometrical considerations that silicon recoil nuclei have a very low probability (by direct impact and/or assisted by diffusion and/or junction funneling) to induce at least a double cell upset in the circuit since two first neighbor sensitive drain regions are physically separated by a distance larger than this maximum range. Consequently, MCU events detected in the WEST experiment cannot be due to D-D neutron interactions in the silicon (or elsewhere in the back-end-of-line materials) and, consequently, are the signature of higher energetic neutrons, presumably that of D-T neutrons whose presence was qualitatively revealed in the WEST neutron flux by the DIAMON spectrometer (see Fig. 8). To verify this assumption at the circuit level, we carried out Monte Carlo simulations for which results are presented below.

B. TIARA simulations

TIARA Monte Carlo simulations were performed on a matrix of 15×15 SRAM circuits using the 14 Geant4 databases separately computed to generate neutron-silicon interaction events in the simulation volume. A total of 20 simulation runs were performed for each ensemble of events contained in the 14 distinct databases, each database gathering the events obtained for 500 million incident neutrons on a silicon volume of $1\ cm^2 \times 20\ \mu m$. This represents a total of 30.6 millions of simulated events in the SRAM matrix. From these raw data, results of Fig. 14 have been obtained. They show that MCU events effectively occur in significant proportion only for neutrons above 4-5 MeV, thus excluding lower energy neutrons, such as emitted in D-D reactions, in the production process of MCU events. Additionally, the comparison of TIARA results and experimental data reported in Fig. 15 shows that simulations well agree with the measurements at 14 MeV in terms of event multiplicity distributions: the proportion of SBU was measured at 88.5% (LPSC) and 86.6% (IRSN) and simulated at 90.5%, the proportion of MCU(2) is experimentally equal to 5-6% and simulated at 7.3%. The most notable difference has been obtained for MCU(3): simulation estimates an event occurrence around 1.4% but was measured at 6% at GENESIS and at 9.8% at AMANDE. The lack of statistics in experimental data or a weakness of the physical models implemented in TIARA, notably the absence of bipolar amplification modeling, may explain such a difference.

One must recall at this level that MCU events can be triggered by two main mechanisms: a direct effect of the range of secondaries and the bipolar parasitic amplification resulting from the channeling diffusion of minorities carriers in the same well [9]. In this last case, the effect is generally strongly amplified by the presence of an underlying deep Nwell, that reinforces minority carrier channeling in the impacted well. But our device is without deep Nwell and the pattern of the observed MCUs in all measurements shows that these events do not systematically involve the same well for the upset cells. These two facts combined with the good agreement between measurements and TIARA simulation results shown in Fig. 15 thus suggest that the range of secondaries produced in neutron-circuit interaction events play here the decisive role in the occurrence of MCU events, in addition to a limited contribution of the bipolar amplification effect in such a 65nm bulk SRAM [9].

Finally, Fig. 16 compares experimental data and simulation expressed in terms of bit-flip neutron cross-sections, evidenc-

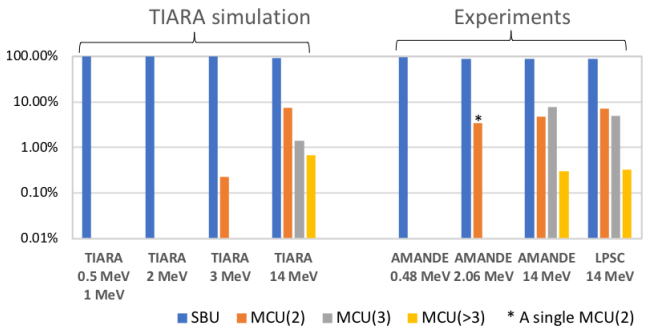

Fig. 15. Comparison between TIARA simulation and experimental results.

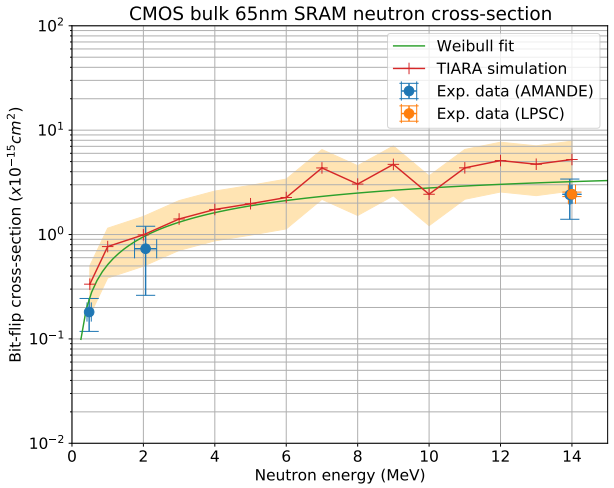

Fig. 16. Neutron cross-section for the CMOS bulk 65 nm SRAM as obtained from monoenergetic measurements at 0.48, 2.45 and 14 MeV and from TIARA simulation. The Weibull fit curve derived from the experimental data is also plotted, as well as the 95% confident interval for Monte Carlo simulation.

ing the good agreement within a factor of 2 between monoenergetic TIARA values and measurements at both AMANDE and GENESIS. The green line corresponds to a fitting of the Weibull function parameters with experimental values:

$$\sigma_n(E) = \sigma_{sat}\left\{1 - exp\left[-\left(\frac{E - E_{th}}{\alpha}\right)^{\beta}\right]\right\} \quad (4)$$

with $\sigma_{sat} = 3 \times 10^{-15}\ cm^2/bit$, $E_{th} = 0.119\ MeV$, $\alpha = 8.076$ and $\beta = 0.895$ as plotted in Fig. 16.

The fitting procedure has been developed under Python environment using the scipy.optimize.curve_fit function that uses a non-linear least squares analysis to fit the four parameters of (4) to experimental data [27].

C. Synthesis

From this ensemble of results including both Geant4 and TIARA simulations, we can argue that MCU events are due to higher energy neutrons than those produced in D-D fusion reactions. These neutrons should be very certainly the so-called triton burn up neutrons produced in the D-T fusion reaction, and/or possibly the photoneutrons produced during a disruption event occurring at the end of a machine shot. Such disruptions were therefore rare during this C5 campaign and only occurred in 10-15% of the machine shots. In order to evaluate the proportion of D-T neutrons produced during the deuterium shots, we first considered the occurrence of MCU events experimentally measured: at LPSC, for a total neutron fluence of $7.45 \times 10^7\ n/cm^2$, the real-time setup detected a total of 60 MCU events. The ratio is thus ≈ 8 MCUs for $10^7\ n.cm^{-2}$ of pure 14 MeV neutrons. Similarly, at IRSN, for a total neutron fluence of $4.17 \times 10^7\ n.cm^{-2}$, 37 MCUs were detected. The ratio is in this case equal to ≈ 8.8 MCUs for $10^7\ n.cm^{-2}$. During the WEST experiment, the same ratio can be also evaluated on the whole campaign to enlarge the rather weak statistics of events: 8 MCU events were detected for a total neutron fluence of $5.6 \times 10^8\ n.cm^{-2}$, that gives 0.14 MCUs per $10^7\ n.cm^{-2}$. From these two ratios, we can deduce that the proportion of D-T neutrons in the WEST neutron flux, responsible of the MCU events, should be $\frac{0.14}{8} \times 100 \approx 1.75\%$ when considering LPSC data (respectively $\frac{0.14}{8.8} \times 100 \approx 1.60\%$ when considering IRSN data). This value is on the order of magnitude of the ratio generally reported between D-T and D-D neutron yields from deuterium plasmas in tokamak experiments [17]. In the present case, for WEST tokamak, this ratio is close to the ratio $\frac{1}{200} \approx 0.5\%$ generally observed for the combination of these geometry, confinement and experimental conditions [28]. The overestimation of this ratio may be primarily due to the unverified hypothesis that the contribution of photoneutrons is negligible in the production of MCU events. Also the neutron metrology and the relatively weak MCU statistics obtained for the whole C5 campaign may also have a significant impact on this rough estimation which remains realistic in its order of magnitude.

V. Implications for ITER electronics reliability

The results obtained in this first study allow us to consider two types of projections for ITER, the future power fusion experimental reactor, in terms of reliability of its electronics:

1) The first one concerns the expected reliability level of the electronics during the machine commissioning phase. Although WEST only experiences D-D plasma, the neutron flux experienced during machine operation at WEST mimics in terms of energy spectrum the ITER radiation environment that will be supported during D-D plasma tests of the machine. These tests are scheduled during its commissioning phase after 2035. Of course, the difference in the volumes of the plasma chamber, respectively 50 m^3 for WEST against 840 m^3 for ITER, leads to an important reduction factor in terms of neutron flux in the vicinity of the WEST tokamak with respect to ITER [29]. On the basis of our experimental results revealing the key-role of higher energy neutrons than D-D neutrons in the production of MCU events, the soft error rate of a given digital circuit subjected to the ITER conditions during D-D tests and in the vicinity

of the tokamak should be now more precisely estimated by numerical simulation considering: 1) the flux amplification factor of ITER with respect to WEST, 2) the proportion of "high energy" neutrons in the total ITER neutron flux, and 3) the exact geometrical dimensions of the ITER tokamak in the neutron flux model derived in the Appendix.

2) In addition, the measurement and modeling of the neutron cross section in the [0.5-14 MeV] energy domain, shown in Fig. 16, makes it possible to go further and to give an estimation of the error rate for the nominal operation of ITER in D-T plasma at different locations in the tokamak building. To do this, the knowledge of the neutron flux energy distribution in these locations is necessary and can be achieved, at this level, by a complex numerical simulation of the tokamak building using a radiation transport code. These data, obtained by the ITER radiation calculation group on the quasi definitive superstructure of the building (including all the shielding structures) [30], will be available shortly, opening the door to such SER estimations. Projections concerning the 65 nm SRAM circuit directly derived from the combination of these data with our results of Fig. 16 should be published very soon in a separate paper.

VI. Conclusion

In conclusion, real-time measurements of single-event upsets during a D-D fusion experiment conducted at WEST tokamak surprisingly evidence the production of MCU events in a 65 nm SRAM test vehicle that cannot be attributed to 2.45 MeV neutrons. Indeed, at this energy, interactions of neutrons with silicon only produce Si recoil nuclei characterized by submicrometer ranges in the bulk material that are not able to induce multiple cell upsets in such a memory technology characterized by a low bipolar amplification effect. Using complementary 14 MeV neutron characterization and soft error rate circuit simulation, we highlighted the non-negligible role of higher energy neutrons, possibly 14 MeV neutrons produced in triton burn up during deuterium discharges. Despite their relative low flux which has been estimated to only represent about 1.7% of the neutron machine production, this flux can quantitatively explain the occurrence of the MCU event distribution detected during the WEST experiment. The present results have been obtained on a mature technology that is not entirely representative of current and future ultra-scaled bulk technologies typically below 20 nm. These latter are characterized by smaller transistor/cell dimensions and smaller critical charges for SRAMs. Roughly, they are expected to be more sensitive to neutron-induced secondaries, both at 2.45 MeV and at 14 MeV, and to present an increased rate of multiple cell upsets with larger size events. So, the results obtained in this study on a 65 nm bulk SRAM clearly do not correspond to a worst case and they should encourage the greatest vigilance for future technologies used in the radiative environment of fusion machines.

For a given circuit and putting aside the question of its possible sensitivity to thermal neutrons, the knowledge of its neutron cross-section in the particular energy domain [0.5-14 MeV], a domain usually not covered by standard neutron tests as performed for atmospheric or ground level qualification, appears to be an essential prerequisite to anticipate its reliability in the radiation environment of future fusion machines. A future qualification method for ITER's electronics could be based on such a systematic characterization for the most important components and circuits concerning the operation of the machine.

Appendix

During the WEST experiment, the neutron fluence (cm^{-2}) at the level of our test bench located in the experimental hall (position P_3, see Fig. 4) has been estimated from the response of three groups of fission chambers positioned at 120° around the tokamak vaccum chamber and integrating the total number of neutrons N_e produced in the whole tokamak chamber during a machine shot. From the quantities defined in Fig. 4 and considering the tokamak chamber as a uniform and isotropic source of neutrons, the neutron flux $d\phi$ emitted from an elementary sector of volume $dV = \pi r^2 R d\alpha$ and passing through the top face of the memory circuits is:

$$d\phi = N_e \times \frac{dV}{V_T} \times \frac{cos(\beta)}{4\pi d^2} \tag{5}$$

with $dV = \pi r^2 R d\alpha$, $V_T = 2\pi^2 r^2 R$ is the volume of the toroidal tokamak chamber and d is the distance separating the center of the elementary sector and point P_3. We have:

$$d^2 = (L - R\cos(\alpha))^2 + (R\sin(\alpha))^2 \tag{6}$$

$$\cos(\beta) = \frac{L - R\cos(\alpha)}{d} \; with \; L > R \tag{7}$$

Finally:

$$\phi = \frac{N_e}{4\pi^2} \times \int_0^{\pi} \frac{cos(\beta) d\alpha}{d^2} \tag{8}$$

which can be numerically evaluated. Note that if $L >> R$, the integral term reduces to π/L^2 and $\phi = \frac{N_e}{4\pi L^2}$ that corresponds to the expression of a point source located at O.

Acknowledgment

The authors sincerely thank M. Baylac and B. Cheymol from the Laboratoire de Physique Subatomique et de Cosmologie (Université Grenoble-Alpes, CNRS/IN2P3) for providing free access to the GENESIS platform. The authors also thank all the technical staff of the WEST tokamak facility for their technical support during all the irradiation campaign. Finally, the technical assistance of R. Babut from the Institut de radioprotection et de sûreté nucléaire (IRSN) for near real-time neutron spectroscopy and access to the AMANDE irradiation facility platform is sincerely acknowledged.

ITER disclaimer

The views and opinions expressed herein do not necessarily reflect those of the ITER Organization.

REFERENCES

[1] E. Morse, *Nuclear Fusion*. Cham (Switzerland): Springer Nature Switzerland AG, 2018.

[2] J. Wesson, *Tokamaks, fourth edition*. Oxford: Oxford Science Publication, 2011.

[3] D. Munteanu and J.L. Autran, "Modeling of digital devices and ICs submitted to transient irradiations," *IEEE Trans. Nucl. Sci.*, Vol. 55, no. 4, pp. 1854-1878, Sept. 2008.

[4] A.J.N. Batista, C. Leong, B. Santos, A. Fernandes, A.R. Ramos, J.P. Santos, J.G. Marques, J.P. Teixeira and B. Gonçalves, "Test results of an ITER relevant FPGA when irradiated with neutrons," in *2015 Int. Conf. Adv. Nucl. Instrum. Meas. Methods Appl.*, Lisbon, Portugal, 2015, pp. 480-483.

[5] A.J.N. Batista, C. Leong, B. Santos, A. Fernandes, A.R. Ramos, J.P. Santos, J.G. Marques, I.C. Teixeira, J.P. Teixeira, J. Sousa and B. Gonçalves, "SEU mitigation exploratory tests in a ITER related FPGA," *Fusion Eng. Des.*, Vol. 118, no. 5, pp. 111-116, May 2017.

[6] J.L. Autran, P. Roche, S. Sauze, G. Gasiot, D. Munteanu, P. Loaiza, M. Zampaolo, and J. Borel, "Altitude and Underground Real-Time SER Characterization of CMOS 65 nm SRAM," *IEEE Trans. Nucl. Sci.*, Vol. 56, no. 4, pp. 2258-2266, Aug. 2009.

[7] J.L. Autran, D. Munteanu, S. Sauze, G. Gasiot, and P. Roche, "Altitude and Underground Real-Time SER Testing of SRAMs Manufactured in CMOS Bulk 130, 65 and 40 nm," in *IEEE Radiat. Effects Data Workshop*, Paris, France, 2014, pp. 9-16.

[8] J.L. Autran, D. Munteanu, S. Moindjie, T. Saad Saoud, S. Sauze, G. Gasiot, and P. Roche, "ASTEP (2005-2015) : Ten Years of Soft Error and Atmospheric Radiation Characterization on the Plateau de Bure," *Microelectron. Rel.*, Vol. 55, no. 9-10, pp. 1506-1511, Sept. 2015.

[9] D. Giot, P. Roche, G. Gasiot, J.L. Autran and R. Harboe-Sorensen, "Heavy Ion Testing and 3-D Simulations of Multiple Cell Upset in 65 nm Standard SRAMs," *IEEE Trans. Nucl. Sci.*, Vol. 55, no. 4, pp. 2048-2054, Aug. 2008.

[10] S. Moindjie, J.L. Autran, D. Munteanu, G. Gasiot, and P. Roche, "Multi-Poisson process analysis of real-time soft-error rate measurements in bulk 65 nm and 40 nm SRAMs," *Microelectron. Rel.*, Vol. 76-77, no. 9-10, pp. 53-57, Sept. 2017.

[11] JESD89B (2021, Dec. 14) *Measurement and reporting of alpha particle and terrestrial cosmic ray induced soft errors in semiconductor devices* $[online]$. Available: https://www.jedec.org/standards-documents/docs/jesd-89a

[12] WEST (2021, Dec. 14) *W Environment in Steady-state Tokamak* $[online]$. Available: http://irfm.cea.fr/en/west/

[13] J. Bucalossi, M. Missirlian, P. Moreau, F. Samaille, E. Tsitrone, D. van Houtte, T. Batal, C. Bourdelle, M. Chantant, Y. Corre, X. Courtois, L. Delpech, L. Doceul, D. Douai, H. Dougnac, F. Faïsse, C. Fenzi, F. Ferlay, M. Firdaouss, L. Gargiulo, P. Garin, C. Gil, A. Grosman, D. Guilhem, J. Gunn, C. Hernandez, D. Keller, S. Larroque, F. Leroux, M. Lipa, P. Lotte, A. Martinez, O. Meyer, F. Micolon, P. Mollard, E. Nardon, R. Nouailletas, A. Pilia, M. Richou, S. Salasca, and J.M. Travère, "The WEST project: Testing ITER divertor high heat flux component technology in a steady state tokamak environment," *Fusion Eng. Des.*, Vol. 89, no. 9-10, pp. 907-912, Oct. 2014.

[14] ITER (2021, Dec. 15) *Unlimited energy* $[online]$. Available: http://www.iter.org

[15] A. Pola, D. Rastelli, M. Treccani, S. Pasquato, and D. Bortot, "DIAMON: A portable, real-time and direction-aware neutron spectrometer for field characterization and dosimetry," *Nucl. Instrum. Methods. Phys. Res. A*, Vol. 969, no. 7, Art. no. 164078, Jul. 2020.

[16] LPSC (2021, Dec. 14) *About the GENESIS facility* $[online]$. Available: https://lpsc.in2p3.fr/index.php/en/peren-energie-nucleaire/presentation-genesis

[17] H. Sjöstrand, G. Gorini, S. Conroy, G. Ericsson, L. Giacomelli, H. Henriksson, A. Hjalmarsson, J. Källne, D. Palma, S. Popovichev, M. Tardocchi, and M. Weiszflog, "Triton burn-up neutron emission in JET low current plasmas," *J. Phys. D*, Vol. 41, no. 11, Art. no. 115208, Nov. 2008.

[18] E. Nilsson, "Dynamics of runaway electrons in tokamak plasmas," *Ph.D. dissertation*, Ecole Polytechnique, France, 2015.

[19] S. Serre, S. Semikh, S. Uznanski, J.L. Autran, D. Munteanu, G. Gasiot, and P. Roche, "Geant4 Analysis of n-Si Nuclear Reactions From Different Sources of Neutrons and Its Implication on Soft-Error Rate," *IEEE Trans. Nucl. Sci.*, Vol. 59, no. 4, pp. 714-722, Aug. 2012.

[20] D. Munteanu and J.L. Autran, "Susceptibility of Group-IV and III-V Semiconductor-based Electronics to Atmospheric Neutrons Explored by Geant4 Numerical Simulations," *in "Numerical Simulations in Engineering and Science,"* S.P. Rao, Ed. London: IntechOpen, 2017, pp. 234-255.

[21] J.L. Autran and D. Munteanu, "Atmospheric Neutron Radiation Response of III-V Binary Compound Semiconductors," *IEEE Trans. Nucl. Sci.*, Vol. 67, no. 7, pp. 1428-1435, Jul. 2020.

[22] S. Agostinelli et al., "Geant4 – a simulation toolkit," *Nucl. Instrum. Methods. Phys. Res. A*, Vol. 506, no. 3, pp. 250-303, Jul. 2003.

[23] J. Allison, K. Amako, J. Apostolakis, P. Arce, M. Asai et al., "Recent developments in Geant4," *Nucl. Instrum. Methods. Phys. Res. A*, Vol. 835, no. 11, pp. 186-225, Nov. 2016.

[24] P. Roche, G. Gasiot, J.L. Autran, D. Munteanu, R.A. Reed, and R.A. Weller, "Application of the TIARA Radiation Transport Tool to Single Event Effects Simulation," *IEEE Trans. Nucl. Sci.*, Vol. 61, no.3, p. 1498-1500, May 2014.

[25] T. Thery, G. Gasiot, V. Malherbe, J.L. Autran, and P. Roche, "TIARA: Industrial Platform for Monte Carlo Single-Event Simulations in Planar Bulk, FD-SOI, and FinFET," *IEEE Trans. Nucl. Sci.*, Vol. 68, no. 5, pp. 603-610, Apr. 2021.

[26] J.L. Autran and D. Munteanu, *Soft Errors: from particles to circuits*. Oxfordshire: Taylor & Francis, CRC Press, 2015.

[27] scipy.optimize.curve_fit (2021, Dec. 16) *Use non-linear least squares to fit a function, f, to data.* $[online]$. Available: https://docs.scipy.org/doc/scipy/reference/generated/scipy.optimize.curve_fit.html

[28] CEA IRFM, private communication.

[29] L. Bertalot, R. Barnsley, V. Krasilnikov, P. Stott, A. Suarez, G. Vayakis, and M. Walsh, "Fusion Power measurement at ITER," *IEEE Trans. Nucl. Sci.*, Vol. 63, no. 3, pp. 1682-1687, Jun. 2016.

[30] R. Juarez, G. Pedroche, M. J. Loughlin, R. Pampin, P. Martinez, M. De Pietri, J. Alguacil, F. Ogando, P. Sauvan, A. J. Lopez-Revelles, A. Kolšek, E. Polunovskiy, M. Fabbri, and J. Sanz, "A full and heterogeneous model of the ITER tokamak for comprehensive nuclear analyses," *Nat. Energy*, Vol. 6, no. 1, pp. 150–157, Jan. 2021.